Quaternary Science Reviews 87 (2014) 60–69

Contents lists available at ScienceDirect

Quaternary Science Reviews

journal homepage: www.elsevier.com/locate/quascirev

The sea-level fingerprints of ice-sheet collapse during interglacial periods

Carling Hay [a,*], Jerry X. Mitrovica [a], Natalya Gomez [a], Jessica R. Creveling [b], Jacqueline Austermann [a], Robert E. Kopp [c]

[a] Department of Earth & Planetary Sciences, Harvard University, USA
[b] Division of Geological & Planetary Sciences, California Institute of Technology, USA
[c] Department of Earth & Planetary Sciences and Rutgers Energy Institute, Rutgers University, USA

ARTICLE INFO

Article history:
Received 31 July 2013
Received in revised form
18 December 2013
Accepted 20 December 2013
Available online 28 January 2014

Keywords:
Interglacials
Sea level
Fingerprinting
Ice sheets
Sea-level highstands

ABSTRACT

Studies of sea level during previous interglacials provide insight into the stability of polar ice sheets in the face of global climate change. Commonly, these studies correct ancient sea-level highstands for the contaminating effect of isostatic adjustment associated with past ice age cycles, and interpret the residuals as being equivalent to the peak eustatic sea level associated with excess melting, relative to present day, of ancient polar ice sheets. However, the collapse of polar ice sheets produces a distinct geometry, or fingerprint, of sea-level change, which must be accounted for to accurately infer peak eustatic sea level from site-specific residual highstands. To explore this issue, we compute fingerprints associated with the collapse of the Greenland Ice Sheet, West Antarctic Ice Sheet, and marine sectors of the East Antarctic Ice Sheet in order to isolate regions that would have been subject to greater-than-eustatic sea-level change for all three cases. These fingerprints are more robust than those associated with modern melting events, when applied to infer eustatic sea level, because: (1) a significant collapse of polar ice sheets reduces the sensitivity of the computed fingerprints to uncertainties in the geometry of the melt regions; and (2) the sea-level signal associated with the collapse will dominate the signal from steric effects. We evaluate these fingerprints at a suite of sites where sea-level records from interglacial marine isotopes stages (MIS) 5e and 11 have been obtained. Using these results, we demonstrate that previously discrepant estimates of peak eustatic sea level during MIS5e based on sea-level markers in Australia and the Seychelles are brought into closer accord.

1. Introduction

The geological record of past sea level, defined to be the difference between the sea surface and solid surface, can be used to estimate total ice volume (or, equivalently, globally averaged "eustatic" sea level) during interglacial periods. This record can thus provide insight into the stability of polar ice sheets in our progressively warming world. Recent studies have, for example, examined ancient sea-level markers dated to the mid-Pliocene climate optimum at ~3 Ma (Dowsett and Cronin, 1990; Raymo et al., 2011; Miller et al., 2012; Rowley et al., 2013) and past interglacial stages, including Marine Isotope Stage (MIS) 5e at ~120 ka (i.e., the Last Interglacial; Hearty et al., 2007; Kopp et al., 2009, 2013; Dutton and Lambeck, 2012; Muhs et al., 2012) and MIS11 at ~400 ka (McMurtry et al., 2007; Olson and Hearty, 2009; van Hengstum et al., 2009; Bowen, 2010; Muhs et al., 2012; Raymo and Mitrovica, 2012; Roberts et al., 2012).

A complication in such studies is the issue of how ancient sea-level markers at a specific site relate to eustatic sea level. In this regard, before any local observation of ancient sea level can be interpreted to result from changes in ice volumes, the geological indicators need to be corrected for the perturbations in sea level associated with late Pleistocene glacial cycles. This process is known as glacial isostatic adjustment, or simply GIA (Lambeck and Nakada, 1992; Lambeck et al., 2011; Raymo et al., 2011; Dutton and Lambeck, 2012; Raymo and Mitrovica, 2012; Roberts et al., 2012).

This point is well illustrated by studies of sea level during MIS11 at Bermuda and Bahamas. Geological records from these localities suggest that peak sea level at these localities reached ~20 m above the present level during MIS11, and these observations have been variously interpreted as reflecting a major collapse of polar ice sheets (Hearty et al., 1999) or deposition from a mega-tsunami (McMurtry et al., 2007). Raymo and Mitrovica (2012) demonstrated that both sites were contaminated by a large GIA signal

* Corresponding author.
E-mail address: carlinghay@fas.harvard.edu (C. Hay).

0277-3791/$ – see front matter © 2014 Elsevier Ltd. All rights reserved.
http://dx.doi.org/10.1016/j.quascirev.2013.12.022

since they are located on the peripheral bulge of the Laurentide Ice Sheet. A numerical correction for this signal, in which ice volumes during MIS11 were fixed to present-day values, yielded residual sea-level highstands of 6–13 m, where the range incorporates observational error and uncertainty in the correction for GIA and tectonic effects. Raymo and Mitrovica (2012) adopted this range as their estimate for MIS11 eustatic sea level. This estimate is consistent with independent inferences of peak eustatic sea level during MIS11 based on coral reef terraces in Curaçao (Muhs et al., 2012; a preferred range of 8.3–10.0 m) and shoreline deposits from the southern margin of South Africa (Roberts et al., 2012; 13 ± 2 m).

Using a similar methodology, Dutton and Lambeck (2012) focused on MIS5e records in Western Australia and the Seychelles, both regions of relative tectonic stability. They applied numerical GIA corrections to each of these records, where the ice distribution during the last interglacial was fixed to the present-day value, and they obtained residual sea-level highstands of 5.5 m and 9 m, respectively. These values define the bounds on their estimate of peak eustatic sea level during MIS5e (5.5–9 m).

The question arises: If GIA effects have been accurately removed, does the residual signal provide an accurate measure of eustasy, as has been assumed in most previous work (e.g., Dutton and Lambeck, 2012; Raymo and Mitrovica, 2012; Roberts et al., 2012)? The GIA correction in these studies fixed interglacial ice volumes to present day values in order that any residual sea-level signals reflect excess melt during the interglacial (i.e., melt in excess of present-day ice volumes). [One exception is the work by Kopp et al. (2009, 2013). In these studies, the authors used a version of the same geophysical model employed in this paper to assess the covariance between local sea levels and mean global sea level across a range of possible ice-sheet histories. Therefore, the Kopp et al. (2009, 2013) results should not be affected by this assumption of eustasy.] Thus, the question we are asking is whether excess melting of ice sheets and glaciers leads to a uniform change in sea level. In fact, it is well understood that the melting of individual ice sheets and glaciers over time scales of centuries to millennia will drive perturbations to the Earth's gravitational field, solid surface elevation and rotational state, and that these effects combine to produce large geographic variations in sea level (Clark and Lingle, 1977; Clark and Primus, 1987; Conrad and Hager, 1997; Mitrovica et al., 2001; Plag and Jüttner, 2001; Tamisiea et al., 2001). Patterns of sea-level change are distinct for each ice sheet, and thus the geometries have come to be known as sea-level fingerprints.

Fingerprinting is a standard tool for analyzing modern sea-level records because the geographic variability of sea-level change provides a method for determining the sources of meltwater (Mitrovica et al., 2001; Plag and Jüttner, 2001; Hay et al., 2012). However, several notable complications arise for cases in which the melt rate is on the order of 1 mm/yr. First, the melt fingerprint for a given ice sheet is sensitive to the geometry of melting within that ice sheet (Mitrovica et al., 2011). Second, both steric effects (e.g., salinity changes and ocean thermal expansion) and dynamic effects (e.g., ocean circulation changes) are uncertain and may dominate the observed variability (Cazenave and Llovel, 2010; Kopp et al., 2010).

There are indications that such complexities would be less significant in analyzing sea level during interglacials such as MIS5e and MIS11, periods for which there is consensus that both the WAIS and GIS experienced significant mass loss (Kopp et al., 2009, 2013; Dutton and Lambeck, 2012; Muhs et al., 2012; Raymo and Mitrovica, 2012; Roberts et al., 2012). Mitrovica et al. (2011) showed, for example, that the normalized sea-level fingerprint for cases in which either the entire WAIS collapsed or only the marine-based sectors of the WAIS collapsed are essentially identical. Moreover, Kopp et al. (2010) demonstrated that sea-level fingerprints dominate steric and dynamic effects in most events when Greenland melt exceeds ~0.2 m of eustatic sea-level rise, a threshold far lower than the peak sea level obtained during MIS5e and MIS11. Finally, modeling by McKay et al. (2011) suggests that the contribution to eustatic sea level from ocean thermal expansion during MIS5e was less than ~0.5 m. While this bound is preliminary, it implies that the >6 m high stand inferred by Kopp et al. (2009) and Dutton and Lambeck (2012) must have involved major ice-sheet loss.

In this paper we derive the fingerprints associated with the collapse of the WAIS, GIS, and marine-based sectors of the EAIS. We explore the sensitivity of these fingerprints to variations in both the geometry and duration of the ice-sheet collapse. Next, we use these fingerprints in three related applications. First, we identify regions in which the local change in sea level due to ice-sheet collapse would have exceeded the global average value (i.e., eustatic) regardless of the source, or sources, of the meltwater (i.e., WAIS, EAIS, and/or GIS). Second, we compute the value of the three fingerprints at sites considered in previous analyses of peak eustatic sea level during either MIS5e or MIS11. This exercise highlights the geographic variability of the sea-level signal and it provides values necessary for future efforts to fingerprint the sources of interglacial meltwater flux. Finally, we revisit previous estimates of peak eustatic sea level to assess the extent to which they may have been biased by the assumption that GIA-corrected sea-level records are equivalent to eustatic sea level.

2. Methods

Our sea-level predictions are based on a gravitationally self-consistent sea-level theory (Kendall et al., 2005) that accounts for the migration of shorelines associated with local sea-level variations and changes in the extent of grounded, marine-based ice. The theory also incorporates the feedback of Earth rotation perturbations into sea level, where these perturbations are predicted following the rotational stability theory of Mitrovica et al. (2005). The accurate treatment of these effects is essential for robust modeling of fingerprints in the case of major ice-sheet collapse. We will return to this point below.

The sea-level theory used in this study incorporates deformations of a 1-D (i.e., depth varying), self-gravitating, elastically compressible Maxwell viscoelastic Earth model. The density and elastic structure of the model are adopted from the seismic model PREM (Dziewonski and Anderson, 1981). In solving the governing "sea-level equation" we use the pseudo-spectral algorithm described in detail by Kendall et al. (2005) with a truncation at spherical harmonic degree and order 512.

We model polar ice-sheet collapse as a linear change in ice volume that takes place over some time interval ΔT, and we consider scenarios in which ΔT varies from 0 ka (i.e., instantaneous collapse) to 3 ka. This range is consistent with recent analyses of sea-level records from both MIS5e (Blanchon et al., 2009; O'Leary et al., 2013) and MIS11 (Raymo and Mitrovica, 2012) that suggest that these interglacials were characterized by late stage collapse of polar ice sheets. In all calculations, the fingerprints we plot represent the total sea-level change across the interval ΔT. In the case where $\Delta T = 0$, the computed fingerprints are only sensitive to the elastic and density structure of the Earth. A sensitivity to mantle viscosity is introduced when the duration of the collapse exceeds the Maxwell time of the Earth (several centuries to a millennium, depending on the viscosity model). In this regard, our standard calculation adopts an Earth model with a lithospheric thickness of 100 km and uniform upper and lower mantle viscosities of 5×10^{20} Pa s and 10^{22} Pa s, respectively, where the boundary between the latter two regions is at the density discontinuity at

670 km depth in PREM. This model (henceforth "LM") is amongst the class of models best supported by prior analyses of GIA observations (Lambeck et al., 1998; Mitrovica and Forte, 2004); however, we will also consider the sensitivity of the predictions to this choice.

"Eustatic sea level" (ESL) change is loosely defined as the volume of meltwater divided by the area of the ocean. In the case where shorelines are not assumed to be steep vertical cliffs (i.e., where the area of the oceans changes as water is added or removed), a more precise definition of ESL change is the change in the elevation of the sea surface if meltwater were to fill the oceans uniformly. (This definition is analogous to the change in the height of water within a bathtub with sloping walls.) However, in considering the collapse of marine-based ice sheets, the definition of ESL change must be extended to account for meltwater that fills in these marine sectors as they are exposed (Gomez et al., 2010). In this case, we define the ESL change as the uniform change in the height of the sea surface (or sea level, since the solid Earth is assumed to be non-deforming in defining eustasy) after all holes exposed by retreating marine-based sectors are filled. This definition, illustrated schematically in Fig. 1, is consistent with usage in the literature since any sea-level rise observed at sites at distance from the polar ice sheets reflects the redistribution of meltwater after any accommodation space created by retreating, marine-based ice is filled.

We follow Gomez et al. (2010) and normalize the computed fingerprints using the ESL change associated with the modeled melt event. This is appropriate because the computed sea-level change is very nearly linearly related to the ESL change associated with the ice-sheet collapse. That is, the sea-level change at a given location predicted for an ice-sheet collapse with an associated ESL change of 2 m will be very close to half the sea-level change predicted for a collapse of the same ice sheet with an associated ESL change of 4 m (provided that the location is outside of the region where melting occurs, which is the case for sites considered here). Moreover, the total sea-level change due to the collapse of multiple ice sheets will be the sum of the normalized fingerprints for each ice sheet, weighted by the ESL change associated with each.

In the calculations below, we assume that bedrock topography is the same as at present. This assumption has negligible impact on the normalized sea-level fingerprints we present for the two sectors of the Antarctic Ice Sheet and the Greenland Ice Sheet since the normalization depends only on meltwater volume in excess of the marine-based accommodation space. However, it is important to keep in mind that translating an estimate of peak interglacial eustatic sea level into total ice volume will depend on the bedrock topography and shoreline position (as well as the appropriate GIA correction) at the time of the ice-sheet collapse. The marine-based accommodation space for meltwater will be largest at the onset of a given interglacial and smallest at the end of the interglacial. Therefore, ultimately determining the timing of the ice-sheet collapse will be important for converting equivalent eustatic sea level to ice volume.

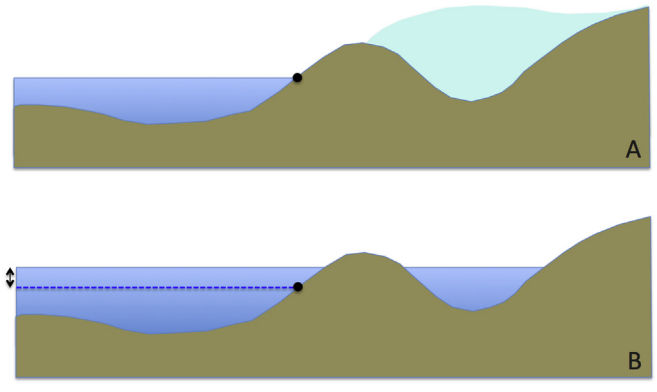

Fig. 1. Schematic illustration of eustatic sea-level change in the event of a collapse of a polar ice sheet with marine-based sectors. The ice sheet, prior to collapse, is shown in panel A. After collapse (panel B), the ESL change is defined as the shift in sea surface height (arrows at left side of frame B) computed by assuming a uniform redistribution of meltwater on a non-deforming Earth where the infill of meltwater into exposed, marine-based sectors of the retreating ice sheet is accounted for.

3. Results

3.1. Normalized sea-level fingerprints

Fig. 2A–C show normalized sea-level fingerprints computed for three scenarios: collapse of the entire WAIS (ESL = 5 m; Mitrovica et al., 2011), the maximum GIS collapse simulation of Stone et al. (2013) (ESL = 3.8 m; see their Fig. 8a, e) and collapse of all marine-based sectors of the EAIS (ESL = 14.2 m), respectively. In each case, we assume rapid ($\Delta T = 0$) collapse of the ice sheet. As discussed above, these fingerprints are normalized by the ESL change associated with each melt event (Fig. 1).

The physics underlying these fingerprints is well understood (e.g., see Mitrovica et al. (2011) for a recent review). In response to the ice-sheet collapse, ocean water migrates away from the melt zone due to both the diminished gravitational attraction of the ice sheet on the ocean and the elastic uplift (rebound) of the mantle and crust. The net effect of these two processes is a zone of sea-level fall close to the melting ice sheet with a maximum amplitude that is approximately an order of magnitude greater than the ESL rise associated with the melt event (these values are off the scale of the color bar used in the figures).

Outside this near-field zone, sea level rises with an amplitude that peaks ~35–40% higher than the ESL value. A variety of processes contribute to the geometry of predicted sea-level change in the far field of a collapsing ice sheet. For example, ocean meltwater loading drives crustal subsidence that peaks well away from continents, and hence the zones of maximum predicted sea-level rise are also located well offshore. The marked azimuthal asymmetry in the fingerprints originates from the off-axis location of the polar ice sheets. There are two reasons for such asymmetry. First, since the polar ice sheets are centered off-axis, the migration of water away from them as their gravitational pull diminishes will not be longitudinally symmetric. Second, and more subtle, an off-axis ice-sheet collapse will perturb the orientation of the Earth's rotation axis (i.e., drive true polar wander, TPW) and the associated perturbation to the centrifugal potential will produce a sea-level signal (Milne and Mitrovica, 1996). In particular, the local rotation axis will reorient toward the zone of ice-sheet collapse (i.e., the South Pole will move toward the WAIS in Fig. 2A and toward the EAIS in Fig. 2C, while the North Pole will move toward the GIS in Fig. 2B), and this will lead to a spherical harmonic degree-two, order-one "quadrential" sea-level perturbation (Milne and Mitrovica, 1996; Gomez et al., 2010). The effect of this quadrential perturbation is significant. As an example, the collapse of the WAIS would lead to TPW of approximately 100 m per meter of ESL change; the sea-level signal driven by this TPW would be responsible for about a third of the predicted sea-level rise above eustatic that is evident offshore of North America's coastlines in Fig. 2A.

3.2. Sensitivity to geometry, melt duration and mantle viscosity

We first consider the sensitivity of the fingerprints to the geometry of the ice-sheet collapse. As discussed in the Introduction,

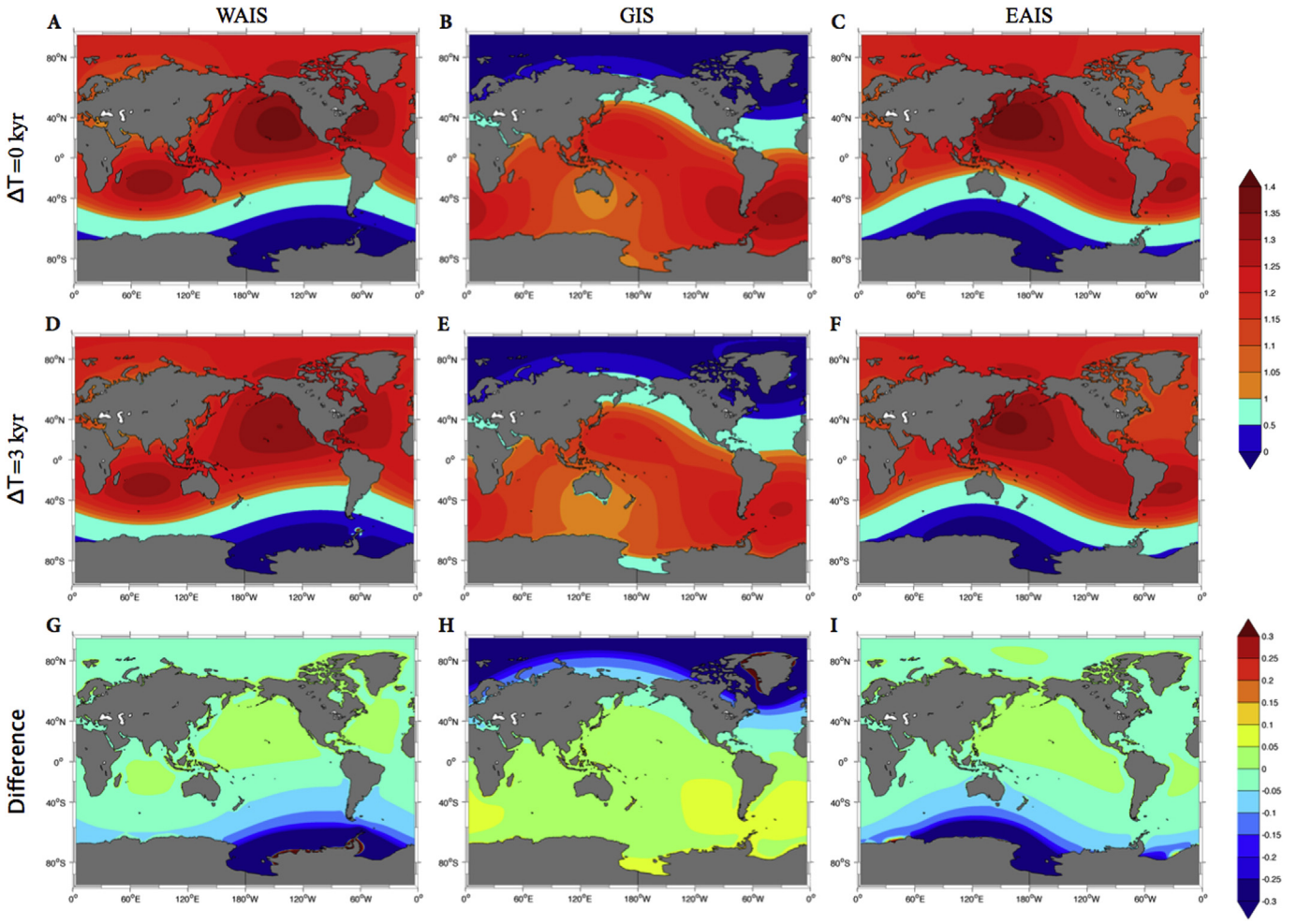

Fig. 2. (A–C) Normalized fingerprints of sea-level change following the rapid collapse of the WAIS, GIS, and EAIS, respectively (i.e., $\Delta T = 0$). In frames (A)–(C) the calculations assume complete collapse of the WAIS, the maximum GIS collapse scenario of Stone et al. (2013), and the collapse of only marine-based sectors of the EAIS, respectively. (D–F) As in (A–C), except that the normalized fingerprints are computed for melt events of duration $\Delta T = 3$ ka. In this case, ice volume is assumed to decrease linearly over the 3 ka melt phase. (G–I) The difference in the predictions based on $\Delta T = 0$ and $\Delta T = 3$ ka simulations (i.e., 2G is 2D minus 2A, etc.). The fingerprints are normalized by the ESL change associated with the melt event (see Fig. 1 and text).

Mitrovica et al. (2011) demonstrated that normalized fingerprints computed assuming either a complete collapse of the WAIS (as in Fig. 2A) or a collapse limited to marine-based sectors of the ice sheet show negligible differences despite the fact that the ESL change associated with the two scenarios, 5.0 m and 3.5 m, respectively, are significantly different. We therefore investigate, in Fig. 3, the sensitivity of the GIS fingerprint to variations in the melt geometry. The normalized fingerprint in Fig. 2B was computed by adopting the maximum GIS collapse simulation for MIS5e of Stone et al. (2013) (ESL = 3.8 m). Fig. 3 shows the difference between this fingerprint and normalized fingerprints based on three alternate GIS collapse simulations discussed by Stone et al. (2013; see their Fig. 8): their "most likely" scenario (ESL = 1.5 m; see their Figs. 8b, f), an alternative scenario with the same amount of melt (ESL = 1.5 m; see their Figs. 8d, h), and their scenario having the minimum excess melt (ESL = 0.4 m; see their Figs. 8c, g). The amplitude of the discrepancies plotted in Fig. 3 is less than 0.05 everywhere except in the very near field of the GIS, and, with the exception of the east coast of Canada and the U.S., the discrepancy is less than 0.02.

Next, we consider the sensitivity of the results to the adopted duration of the ice-sheet collapse. The normalized fingerprints in Fig. 2D–F are analogous to those in Fig. 2A–C, with the exception that ice-sheet melt occurs linearly over the course of 3 ka (i.e., $\Delta T = 3$ ka). Frames 2G–I show the difference between this case and the instantaneous ($\Delta T = 0$) collapse scenarios illustrated in the first row of the figure. In the far field of the melting ice sheet, that is, in the area where sea level is predicted to rise, the normalized fingerprints are markedly insensitive to the adopted duration of the ice-sheet collapse. Consider the case of WAIS collapse (Fig. 2A, D). The global peak sea-level rise is predicted off the west coast of the U.S., and at this location the $\Delta T = 0$ and $\Delta T = 3$ ka simulations yield peak values of 1.38 and 1.36, respectively. Similarly, for the EAIS collapse scenarios (Fig. 2C, F), the sea-level rise is predicted to peak east of Japan, and the $\Delta T = 0$ and $\Delta T = 3$ ka simulations also yield values of 1.38 and 1.36, respectively. Finally, GIS collapse produces a peak sea-level rise of 1.33 in the south Atlantic for the $\Delta T = 0$ simulation (Fig. 2B) and 1.27 for $\Delta T = 3$ ka (Fig. 2E).

Why are the predicted sea-level changes associated with GIS melt somewhat more sensitive to the adopted duration of the collapse than either of the two Antarctic collapse scenarios? The reason is that the simulations prescribe melt as coming primarily from marine sectors in the Antarctic. In this case, the progressive reduction in sea level due to isostatic adjustment in the near field (which acts to moderate the gravitational effects on sea surface height) is partially compensated by the outflux of water from these

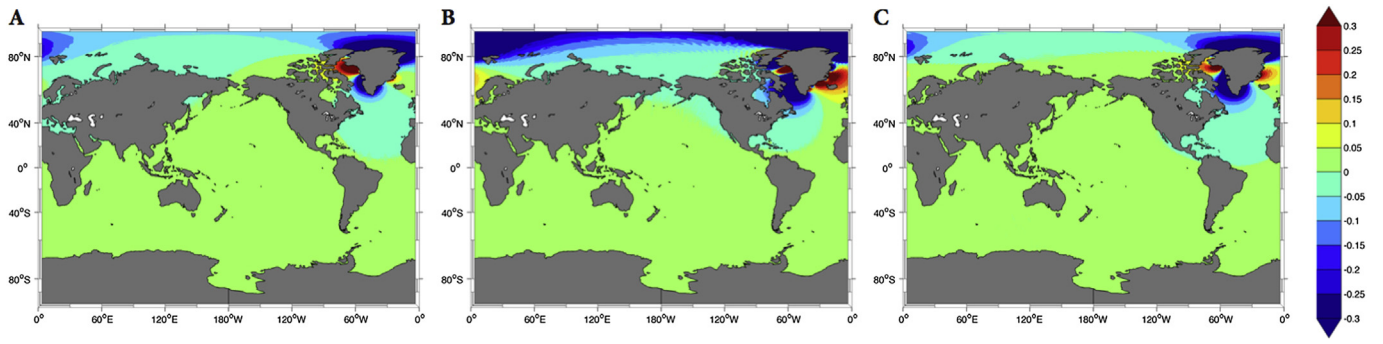

Fig. 3. Difference in the normalized fingerprint of GIS collapse computed using three coupled climate-ice sheet model simulations for MIS5e described by Stone et al. (2013) and the normalized fingerprint for their maximum collapse scenario (Fig. 2b). The three predictions are based on the following GIS collapse scenarios (Stone et al., 2013): (A) the "most likely" simulation; (B) an alternative scenario with the same amount of melt as their "most likely" simulation; and (C) the simulation with the smallest change in GIS volume across MIS5e.

uplifting marine sectors (i.e., removing water from the area previously covered by ice in Fig. 1B; Gomez et al., 2010). A similar compensation does not occur over Greenland.

As we noted above, the simulations for which the duration of the ice-sheet collapse exceeds the Maxwell time of the Earth model are a function of the (uncertain) radial viscosity profile of the mantle. To investigate this issue, we computed the predicted (normalized) sea-level rise at one site, the Seychelles, as a function of the adopted duration of the collapse of the WAIS, EAIS, and GIS using two distinct radial viscosity models (Fig. 4). The solid lines on the figure depict results using the standard Earth model defined above (Lambeck et al., 1998; Mitrovica and Forte, 2004), whereas the dashed lines illustrate the results when we adopt the VM2 viscosity model (Peltier, 2004), which is characterized by a weaker lower mantle viscosity of $2-3 \times 10^{21}$ Pa s. The sensitivity of the predictions to the adopted lower mantle viscosity is small.

3.3. *Identifying regions of greater than global average sea-level rise*

The results in Fig. 4 indicate that any combination of polar ice-sheet collapse during a past interglacial, regardless of the adopted radial viscosity model, would have led to a sea-level rise in the Seychelles that was greater than the ESL change associated with the

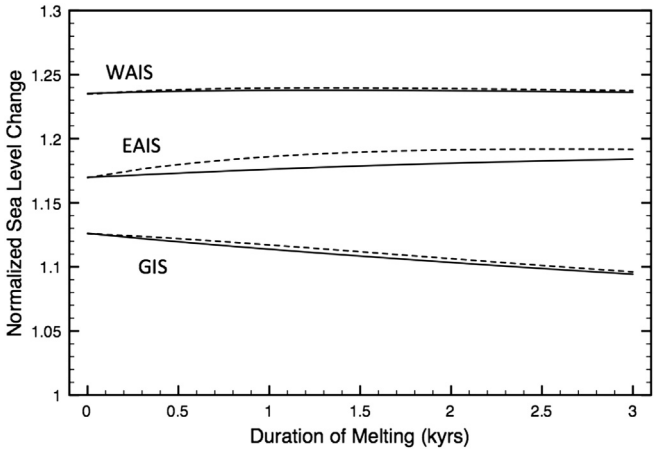

Fig. 4. Predictions of the normalized sea-level rise at the Seychelles as a function of the duration of the modeled ice-sheet collapse. Results are shown for simulations of WAIS, EAIS, and GIS collapse (as labeled), each adopting two different radial profiles of mantle viscosity: the LM model defined in the text (solid lines) and the VM2 viscosity model (dashed lines; Peltier, 2004).

collapse. In this section we extend this idea to identify all sites that would have experienced greater than the global average sea-level rise.

Since it is likely that the WAIS and GIS would have dominated any contribution from the EAIS toward the total excess melting during the MIS5e and MIS11 interglacials (Solomon et al., 2007; Dutton and Lambeck, 2012; Raymo and Mitrovica, 2012), we begin by focusing on the sea-level fingerprints of these two ice sheets. In particular, Fig. 5A uses the fingerprints in Figs. 2A and B to identify all sites that would have had a greater-than-eustatic sea-level rise in the case of rapid collapse of any combination of the WAIS and GIS. The dark red zone on the figure identifies sites for which the predicted sea-level rise is a minimum of 25% greater than both the WAIS and GIS eustatic values. The lighter red identifies sites in which the minimum value for both normalized fingerprints lies between 1.20 and 1.25, the minimum lies in the range 1.15–1.20 for sites in the yellow zone, and so on.

Fig. 5A demonstrates that large areas of the low-latitude oceans must have experienced greater than ESL rise in response to the rapid collapse of the WAIS and GIS during an interglacial, regardless of the relative contributions from these ice sheets to the total meltwater flux. For example, Hawaii experienced a sea-level rise at least 20% greater than the global average. Furthermore, sea-level rise along the eastern shoreline of Japan, across the Philippines and the southern margin of South Africa was at least 15% greater than the global average. As discussed above, these regions of "super-eustatic" sea-level rise are concentrated in relatively low latitudes because a specific fingerprint is characterized by greater-than-eustatic values at large distances from (in the far field of) the collapsing ice sheet, and only low latitude sites are at great distance from both the GIS and WAIS.

The remaining frames of Fig. 5 explore the sensitivity of the results in Fig. 5A to various aspects of the prediction. For example, Fig. 5B is analogous to Fig. 5A, except that the collapse of both the GIS and WAIS is assumed to take place over 3 ka, rather than instantaneously. The results are relatively insensitive to the duration of the collapse, indicating that the regions identified by contouring in Fig. 5A will be characterized by a greater than ESL rise regardless of both the relative contributions from the WAIS and GIS and the duration of the collapse of either ice sheet (up to $\Delta T = 3$ ka). The main difference between Fig. 5A and B is that there is no site identified in the latter where the sea-level rise is guaranteed to be at least 25% greater than the eustatic value.

While there is consensus that the WAIS and GIS are the most susceptible to collapse during periods of ice age warmth, it is possible that the EAIS may have contributed several meters of

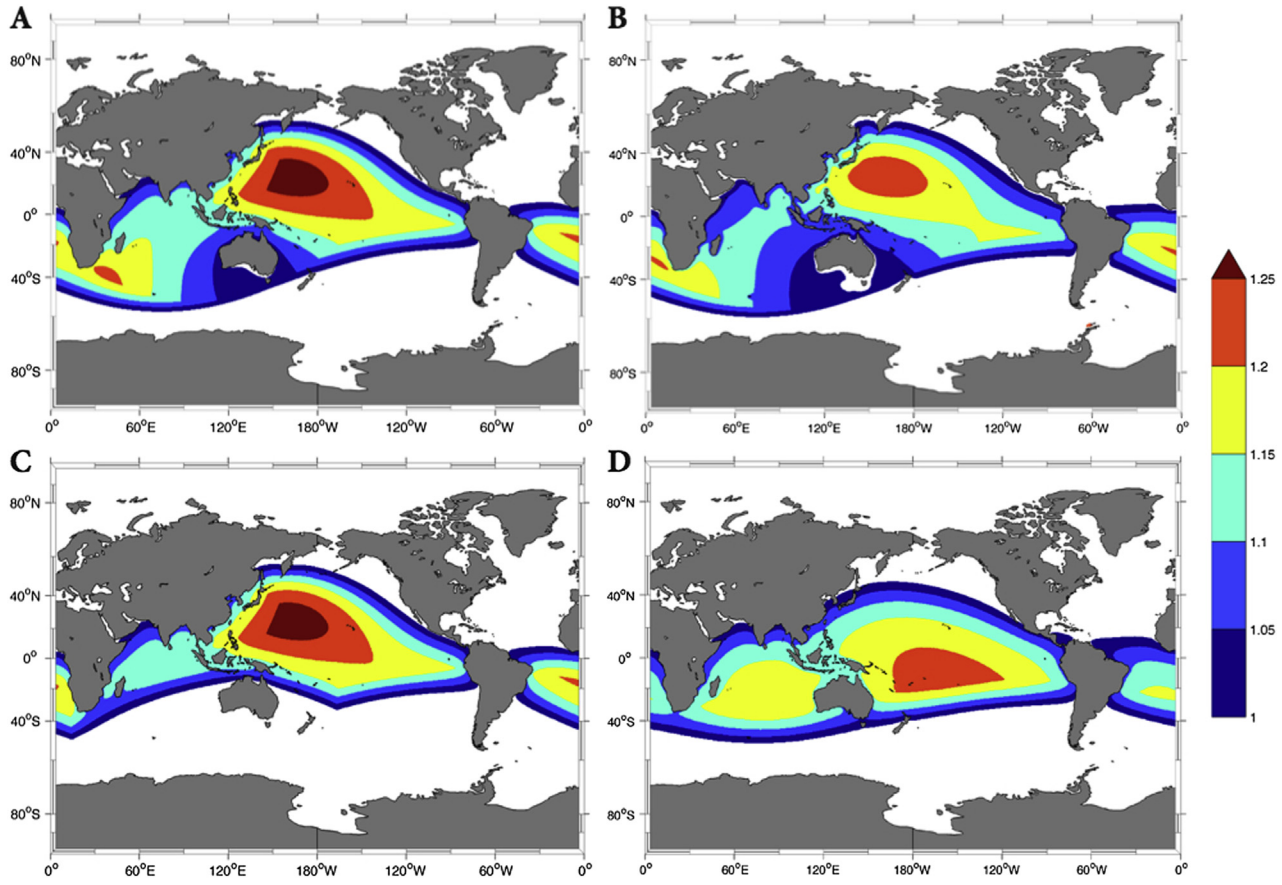

Fig. 5. (A) Contours showing the minimum (normalized) fingerprint value for rapid melting from the WAIS and GIS. That is, the yellow zone shows the locations where the minimum value of the WAIS and GIS fingerprints in Fig. 2A and B, respectively, falls within a range 15–20% greater than the eustatic value. Only sites at which the minimum is greater than the eustatic value (i.e., greater than one for normalized fingerprints) are shown. (B) As in frame (A), except that the analysis is performed for normalized fingerprints in the case of a melt duration 3 ka (as in Fig. 2D and E). (C) As in (A), except we show the minimum value of all three fingerprints (WAIS, GIS, and EAIS). (D) As in frame (A) except the predictions of the normalized fingerprints do not include the signal associated with rotational feedback (see text).

meltwater to peak interglacial highstands (Dutton and Lambeck, 2012; Raymo and Mitrovica, 2012). In Fig. 5C we extend the result in Fig. 5A to include melting from the EAIS. That is, the figure isolates sites which experience some minimum amount of sea-level rise regardless of which of the three polar ice sheets is the source of the melting. In some regions, for example the north Pacific and south Atlantic, inclusion of the EAIS in the analysis has negligible effects on the computed minimum sea-level rise. In contrast, greater-than-eustatic sea-level rise within the Indian Ocean is localized more strongly within the northern section of that ocean when EAIS melt is included in the analysis.

Finally, we turn to an issue related to the sea-level theory. In particular, we repeat the calculation in Fig. 5A except that we remove the feedback of Earth rotation perturbations into the sea-level predictions (Fig. 5D). The main difference is that in the no-TPW feedback case, the sites that are guaranteed to experience greater than global average sea-level rise show less longitudinal dependence and are localized to lower latitudes. This is as expected, given that rotational feedback is responsible for a significant component of the longitudinal dependence of the individual fingerprints, as we discussed in the context of Fig. 2. The change in the geometry between Fig. 5A and D can be important at specific sites. As an example, consider the eastern shore of Japan. When rotational feedback is included in the calculations, the minimum sea-level rise for sites along this coast is 18% greater than the eustatic value. This value falls to only ~6% in the case where this physics is not included. Clearly, any effort to infer peak ESL on the basis of GIA-corrected interglacial highstands must incorporate the physics of rotational feedback (Milne and Mitrovica, 1996).

As a final point, as we discussed in regard to the fingerprints in Fig. 2, regions in which predicted sea-level rise is less than the eustatic value are relatively close to the melting ice sheet. As a consequence, we have found that there are no sites in the global ocean that are guaranteed to experience less than the eustatic value when melting occurs within the WAIS and GIS, or from all three polar ice sheets. That is, there is no site in which, in analogy to Fig. 5, the maximum local sea-level change associated with melting from all three of the polar ice sheets is sub-eustatic.

4. Discussion of site-specific sea-level predictions

In this section we discuss predictions of sea-level change due to polar ice-sheet collapse at specific sites considered in previous analyses of ESL during MIS5e and MIS11. To begin, Table 1 lists the normalized sea-level change at 10 sites for the case of melting from the WAIS, EAIS and GIS, and for melt durations of 0 ka and 3 ka, where predictions for the latter case are given for both the LM and VM2 viscoelastic Earth models. The first seven of the sites (Cooring, Australia to Nome, Alaska) were included in the database of MIS11 records compiled by Bowen (2010). Mossel Bay, on the southern coast of South Africa, is the site of MIS11 age records discussed by Roberts et al. (2012). Finally, the Hearty et al. (1999) analysis of

Table 1
Normalized fingerprints of WAIS, EAIS, and GIS collapse at specific sites considered in published MIS11 studies (Hearty et al., 1999; Bowen, 2010; Roberts et al., 2012) for melt events of duration $\Delta T = 0$ and $\Delta T = 3$ka and Earth models LM and VM2 (see text).

Site (primary source)	$\Delta T = 0$			$\Delta T = 3$ ka LM			$\Delta T = 3$ ka VM2		
	WAIS	EAIS	GIS	WAIS	EAIS	GIS	WAIS	EAIS	GIS
Coorong (Murray-Wallace, 2002)	1.10	0.62	0.98	1.10	0.67	0.93	1.11	0.77	0.92
Curaçao (Lundberg and McFarlane, 2002)	1.22	1.14	0.93	1.21	1.13	0.94	1.19	1.11	0.97
Barbados (Schellmann and Radtke, 2004)	1.25	1.15	0.93	1.26	1.17	0.95	1.25	1.16	1.00
Sumba (Jouannic et al., 1988; Pirazzoli et al., 1993)	1.23	1.07	1.09	1.23	1.10	1.05	1.22	1.12	1.05
Charleston, SC (Cronin, 1981; Cronin et al., 1984)	1.27	1.07	0.67	1.23	1.06	0.69	1.19	1.04	0.78
Rome (Karner and Marra, 1998, 2003; Karner and Renne, 1998)	1.06	1.05	0.55	1.07	1.06	0.60	1.07	1.05	0.71
Nome (Muhs et al., 2004; Kaufman, 1992; Kaufman and Brigham-Grette, 1993; Pushgar et al., 1999)	1.25	1.24	0.69	1.22	1.21	0.71	1.19	1.17	0.79
Mossel Bay (Roberts et al., 2012)	1.16	1.10	1.20	1.15	1.09	1.12	1.16	1.10	1.08
Bermuda (Hearty et al., 1999)	1.32	1.11	0.63	1.30	1.12	0.68	1.29	1.13	0.80
Eleuthera (Hearty et al., 1999)	1.30	1.12	0.81	1.29	1.13	0.84	1.27	1.13	0.91

MIS11 sea level was based on data from Bermuda and Eleuthera, Bahamas.

The (normalized) local sea-level predictions in Table 1 vary significantly for each ice sheet and from site to site. Consider, as an example, sites in the Bowen (2010) analysis for the case of rapid ice-sheet melting. GIS collapse produces a sea-level rise in Rome that is only 55% of the eustatic value (Fig. 2B), while the collapse of the WAIS yields a sea-level rise at Rome that is 6% above the eustatic (Fig. 2A), a difference of roughly a factor of two. As a further numerical example, let us assume that peak ESL was 10 m above present during MIS11, and that this peak was equally partitioned into contributions from both WAIS and GIS collapse. Using the results from Table 1, local sea level at the seven sites in the Bowen (2010) analysis due to this melt scenario would be: 10.4 m, 10.7 m, 10.9 m, 11.6 m, 9.7 m, 8.1 m, and 9.7 m. If, as discussed in the Introduction, one interpreted a local (GIA-corrected) sea-level elevation as being equivalent to ESL, then one would overestimate the eustatic level by 11.6% at Sumba and underestimate it by 19% at Rome. In absolute terms, the difference in the two estimates of eustasy would be 3.5 m (11.6 m versus 8.1 m).

Of course, the error in estimating ESL from a single, GIA-corrected sea-level indicator will depend on the relative contributions of the WAIS, GIS and EAIS to the total meltwater budget. In their analysis of the data compiled by Hearty et al. (1999) from Bermuda and Bahamas, Raymo and Mitrovica (2012) inferred peak local sea levels of 9.4 ± 1 m at Bermuda and 11.1 ± 3.6 m at Bahamas after correction for a preferred model of GIA contamination. Using a suite of such GIA models, they estimated that peak ESL during MIS11 was 6–13 m higher than present. Raymo and Mitrovica (2012) further argued that a peak value within this range almost certainly required substantial contributions from both the WAIS and GIS. It is interesting to note from Table 1 that roughly equivalent contributions from these two ice sheets to the total meltwater release during MIS11 would produce a local sea level at Bermuda and Bahamas that is only a few percent different from the eustatic level (i.e., the average of the normalized fingerprints of WAIS and GIS collapse at these two sites is ~ 1).

In Table 2 we list normalized fingerprint values for sites primarily taken from the Dutton and Lambeck (2012) database of MIS5e sea-level records. All of the observations made in regard to the results in Table 1 also hold for these predictions, most notably the large site and ice sheet-dependent range in the mapping between ESL and local sea level. These results have important implications for the Dutton and Lambeck (2012) conclusion that ESL during MIS5e peaked 5.5–9 m above present level. The upper and lower bounds of this estimate were based on GIA-corrected elevations of corals from the Seychelles and along the coast of Western Australia, respectively. The predictions for Seychelles listed in Table 2 indicate that this upper bound on ESL was overestimated by 15–20%, and should thus be revised downward to 7.5 m. (Note, in this regard, that Seychelles is one of the sites in Fig. 5 where local sea level will significantly exceed ESL regardless of the source of meltwater; see also Fig. 4.) In contrast, the predictions for sites in Western Australia indicate that the lower bound on peak ESL cited by Dutton and Lambeck (2012) was overestimated by $\sim 10\%$ if the WAIS and GIS contributed comparable amounts of meltwater, and closer to 0% (or a slight underestimation) if the EAIS contributed to this total.

5. Final remarks

We conclude that equating GIA-corrected MIS5e and MIS11 highstand elevations with peak eustatic level can introduce a significant bias into estimates of the latter (see Tables 1 and 2). The collapse of polar ice sheets gives rise to distinct geographic patterns of sea-level change, and the physics of these sea-level "fingerprints" must be accounted for in order to accurately map GIA-corrected local highstands into estimates of the eustatic level. As an example, we have highlighted the case of the Seychelles. Our fingerprint analysis suggests that a recent estimate of peak eustatic sea level during MIS5e based on field data from this site (Dutton and Lambeck, 2012) should be lowered from 9 m to 7.5 m, bringing it into closer accord with a second estimate from the same study based on sea-level markers from Western Australia. While the uncertainty inherent to field-based estimates of paleo-sea level (e.g., reef-building corals, wave-cut notches, etc.) may be several meters or more, it is important that future estimates of eustatic sea level do not amplify this measurement error with the systematic bias discussed here.

One advantage of the application of fingerprinting to past interglacial periods of ice-sheet collapse, as opposed to similar analyses of modern sea-level records, is that the associated fingerprints are relatively insensitive to the geometry of the melt region (Fig. 3). Likewise, we have also shown that the fingerprints are insensitive to the time history of the ice-sheet collapse for the specific class of scenarios in which we varied the duration of the collapse from 0 to 3 ka (Figs. 2 and 5). Finally, our results indicate that fingerprint-based estimates of peak ESL during interglacials should include a state-of-the-art sea-level theory in which the feedback of perturbations in Earth rotation into sea level is accurately included.

The fingerprinting methodology provides a framework that allows one to move beyond accurately estimating ESL, which has been the focus of the present study, to constraining the source(s) of the meltwater. The latter has been central to fingerprinting analyses of modern records (e.g., Mitrovica et al., 2001), but the lack of

Table 2
Normalized fingerprints of WAIS, EAIS, and GIS collapse at specific sites, primarily from the Dutton and Lambeck (2012) database, for melt events of duration $\Delta T = 0$ and $\Delta T = 3$ ka and Earth models LM and VM2 (see text). Omitted sites: Grassy Key, Windley Key = Key Largo; Rendezvous Hill = Cave Hill, Barbados; Cayucos = Point Loma, CA; All Oahu sites = Makua Valley, Oahu; La Digue Is. = Curieuse Is., Seychelles; Mowbowra Creek, Vlaming Head, Tantabiddi Bay, Yardie Creek = Cape Range, WA.

Site (primary source)	$\Delta T = 0$			$\Delta T = 3$ ka LM			$\Delta T = 3$ ka VM2		
	WAIS	EAIS	GIS	WAIS	EAIS	GIS	WAIS	EAIS	GIS
Panglao Is., Phillipines (Omura et al., 2004)	1.19	1.23	1.17	1.16	1.20	1.10	1.15	1.18	1.08
Hateruma Is., Japan (Ota and Omura, 1992)	1.15	1.30	1.20	1.17	1.30	1.17	1.17	1.26	1.15
Grape Bay, Bermuda (Muhs et al., 2002b)	1.32	1.11	0.63	1.31	1.12	0.68	1.29	1.13	0.80
Crawl Key, Florida (Muhs et al., 2011)	1.28	1.09	0.76	1.24	1.08	0.77	1.21	1.07	0.85
Key Largo, Florida (Muhs et al., 2011)	1.29	1.12	0.82	1.27	1.13	0.84	1.25	1.12	0.91
Great Inagua Is., Bahamas (Chen et al., 1991)	1.29	1.13	0.85	1.27	1.13	0.87	1.25	1.13	0.94
San Salvador Is., Bahamas (Chen et al., 1991)	1.30	1.13	0.82	1.29	1.14	0.85	1.27	1.13	0.92
Abaco Is., Bahamas (Hearty et al., 2007)	1.30	1.12	0.79	1.29	1.13	0.82	1.27	1.13	0.90
Haiti (Bard et al., 1990)	1.28	1.13	0.87	1.25	1.12	0.88	1.23	1.12	0.94
Cave Hill, Barbados (Speed and Cheng, 2004)	1.25	1.15	0.93	1.26	1.17	0.95	1.25	1.16	1.00
Curaçao (Hamelin et al., 1991)	1.22	1.13	0.93	1.21	1.13	0.94	1.19	1.11	0.96
Point Loma, San Diego (Muhs et al., 2002a)	1.30	1.14	0.91	1.26	1.12	0.90	1.21	1.09	0.93
San Clemente Is., CA USA (Muhs et al., 2002a)	1.31	1.16	0.93	1.28	1.15	0.92	1.24	1.12	0.96
Palos Verdes Hills, LA County (Muhs et al., 2006)	1.30	1.15	0.91	1.25	1.12	0.90	1.21	1.09	0.93
San Nicolas Islands, CA USA (Muhs et al., 2006)	1.32	1.17	0.94	1.30	1.16	0.94	1.25	1.13	0.97
Punta Banda, Baja CA (Muhs et al., 2002a)	1.30	1.15	0.92	1.26	1.13	0.91	1.22	1.10	0.95
Isla de Guadalupe, Baja CA (Muhs et al., 2002a)	1.33	1.19	0.98	1.33	1.20	0.99	1.29	1.17	1.03
Cabo Pulmo, Baja CA (Muhs et al., 2002a)	1.29	1.15	0.96	1.27	1.14	0.95	1.23	1.11	0.98
Xcaret, Yucatan (Blanchon et al., 2009)	1.27	1.13	0.90	1.25	1.12	0.90	1.22	1.11	0.94
Makua Valley, Oahu (Hearty et al., 2007)	1.35	1.33	1.22	1.33	1.31	1.18	1.31	1.27	1.17
Eritrea Red Sea Coast (Walter et al., 2000)	1.04	1.08	0.95	1.04	1.08	0.93	1.03	1.04	0.93
Mururoa atoll, Tuamoto (Camoin et al., 2001)	1.08	1.23	1.19	1.11	1.24	1.14	1.16	1.24	1.13
Huon Peninsula (Esat et al., 1999)	1.22	1.13	1.11	1.19	1.12	1.05	1.17	1.12	1.03
Sumba Island (Bard et al., 1996)	1.23	1.07	1.09	1.23	1.10	1.05	1.22	1.12	1.05
Curieuse Island, Seychelles (Israelson and Wohlfarth, 1999)	1.23	1.17	1.13	1.23	1.18	1.09	1.24	1.19	1.10
Vanuatu (Edwards et al., 1987)	1.21	1.08	1.11	1.21	1.11	1.07	1.23	1.14	1.07
Rottnest Island, WA (Stirling et al., 1995)	1.22	0.72	1.01	1.19	0.77	0.97	1.19	0.85	0.96
Leander Point, WA (Stirling et al., 1995)	1.21	0.77	1.01	1.18	0.81	0.96	1.17	0.88	0.95
Burney Point, WA (Stirling and Esat, 1998)	1.22	0.78	1.02	1.19	0.82	0.96	1.18	0.89	0.96
Cape Cuvier, WA (Stirling and Esat, 1998; Hearty et al., 2007; O'Leary et al., 2008a,b)	1.24	0.87	1.03	1.22	0.91	0.99	1.20	0.97	0.98
Mangrove Bay, WA (Stirling and Esat, 1998)	1.19	0.98	1.02	1.15	0.98	0.96	1.12	0.99	0.94
Foul Bay, WA (McCulloch and Mortimer, 2008)	1.20	0.65	1.01	1.19	0.71	0.97	1.20	0.81	0.97
H-Abrolhos Is., WA (Zhu et al., 1993)	1.24	0.81	1.03	1.23	0.85	0.99	1.22	0.93	0.99
Shark Bay, WA (O'Leary et al., 2008a,b)	1.24	0.85	1.03	1.21	0.89	0.98	1.20	0.95	0.98
Cape Range, WA (Hearty et al., 2007)	1.24	0.91	1.04	1.23	0.95	1.00	1.21	1.00	1.00

sufficiently accurate field data has limited analogous applications to paleo sea levels. There are a few notable exceptions. The first is the suite of studies that have attempted to constrain the source of meltwater pulse 1A using globally distributed records of the sea-level rise across this event (Clark et al., 2002; Deschamps et al., 2012). The second is the collection of studies by Kopp et al. (2009, 2013) who used a model of the total sea-level response to ice-sheet variations (i.e., a model that included signals from both GIA and excess melting) within the Last Interglacial to correct probabilistically for the difference between local and global sea level. Fig. 2 and Tables 1 and 2 provide the information necessary to extend this application of fingerprinting to past interglacials. In this regard, the temporal resolution of sea-level fluctuations within interglacials such as MIS5e is the subject of continuing research. Blanchon et al. (2009) and O'Leary et al. (2013), for example, have argued for a late MIS5e collapse of polar ice on the basis of data from the Yucatan and Western Australia, respectively. In contrast, a statistical analysis of globally distributed records has detected a double peak in ESL across the MIS5e interval (Kopp et al., 2013). These recent advances suggest that a target for future work may be to fingerprint the ice sheets responsible for these interglacial peaks in sea level.

As a final point, the present analysis has focused on sea-level changes during past interglacials MIS5e and MIS11 for which there is strong field evidence of ice-sheet collapse. Our results are, however, also appropriate for millennial-scale projections of sea-level change in a progressively warming world characterized by major ice-sheet collapse.

Acknowledgments

CH, JXM and REK were supported by the National Science Foundation (ARC-1203414 and ARC-1203415). JXM also acknowledges support from Harvard University and the Canadian Institute for Advanced Research. The authors would like to thank the editor and Daniel Muhs for their useful feedback.

References

Bard, E., Hamelin, B., Fairbanks, R.G., 1990. U-Th ages obtained by mass spectrometry in corals from Barbados: sea level during the past 130,000 years. Nature 346, 456.
Bard, E., et al., 1996. Pleistocene sea levels and tectonic uplift based on dating of corals from Sumba Island, Indonesia. Geophys. Res. Lett. 23, 1473.
Blanchon, P., Eisenhauer, A., Fietzke, J., Liebetrau, V., 2009. Rapid sea-level rise and reef back-stepping at the close of the last interglacial highstand. Nature 458, 881–885.
Bowen, D.Q., 2010. Sea level ~400000 years ago (MIS 11): analogue for present and future sea level? Clim. Past 6, 19–29.
Camoin, G., Ebren, P., Eisenhauer, A., Bard, E., Faure, G., 2001. A 300 000-yr coral reef record of sea level changes, Mururoa atoll (Tuamotu archipelago, French Polynesia). Palaeogeogr. Palaeoclimatol. Palaeoecol. 175, 325.
Cazenave, A., Llovel, W., 2010. Contemporary sea level rise. Annu. Rev. Mar. Sci. 2, 145–173.

Chen, J.H., Curran, H.A., White, B., Wasserburg, G.J., 1991. Precise chronology of the last interglacial period: ^{234}U-^{230}Th data from fossil coral reefs in the Bahamas. Geol. Soc. Am. Bull. 103, 82.
Clark, J.A., Lingle, C.S., 1977. Future sea-level changes due to West Antarctic ice sheet fluctuations. Nature 269, 206–209.
Clark, J.A., Primus, J.A., 1987. Sea-level changes resulting from future retreat of ice sheets: an effect of CO_2 warming of the climate. In: Tooley, M.J., Shennan, I. (Eds.), Sea-level Changes. Institute of British Geographers, London, United Kingdom, pp. 356–370.
Clark, P.U., Mitrovica, J.X., Milne, G.A., Tamisiea, M.E., 2002. Sea-level fingerprinting as a direct test for the source of global meltwater pulse 1A. Science 295, 2438–2441.
Conrad, C., Hager, B.H., 1997. Spatial variations in the rate of sea level rise caused by present-day melting of glaciers and ice sheets. Geophys. Res. Lett. 24, 1503–1506.
Cronin, T.M., 1981. Vertical crustal movements Atlantic coastal Plain. Geol. Soc. Am. Bull. 92, 812–833.
Cronin, T.M., Bybell, L.M., Poore, R.Z., Blackwelder, B.W., Liddicoat, J.C., Hazel, J.E., 1984. Age and correlation of emerged pliocene and pleistocene deposits, U.S. Atlantic Coastal Plain. Palaeogeogr. Palaeoclimatol. Palaeoecol. 47, 21–51.
Deschamps, P., Durand, N., Bard, E., Hamelin, B., Camoin, G., Thomas, A.L., Henderson, G.M., Okuno, J., Yokoyama, Y., 2012. Ice-sheet collapse and sea-level rise at the Bølling warming 14, 6000 years ago. Nature 483, 559–564.
Dowsett, H.J., Cronin, T.M., 1990. High eustatic sea level during the middle Pliocene: evidence from the southeastern U.S. Atlantic Coastal Plain. Geology 18, 435–438.
Dutton, A., Lambeck, K., 2012. Ice volume and sea level during the last interglacial. Science 337, 216–219.
Dziewonski, A.M., Anderson, D.L., 1981. Preliminary reference Earth model (PREM). Phys. Earth Planet. Int. 25, 297–356.
Edwards, R.L., Chen, J.H., Ku, T.-L., Wasserburg, G.J., 1987. Precise timing of the last interglacial period from mass spectrometric determination of thorium-230 in corals. Science 236, 1547.
Esat, T.M., McCulloch, M.T., Chappell, J., Pillans, B., Omura, A., 1999. Rapid fluctuations in sea level recorded at huon peninsula during the penultimate deglaciation. Science 283, 197.
Gomez, N., Mitrovica, J.X., Tamisiea, M.E., Clark, P.U., 2010. A new projection of sea level change in response to collapse of marine sectors of the Antarctic Ice Sheet. Geophys. J. Int. 180, 623–634.
Hamelin, B., Bard, E., Zindler, A., Fairbanks, R.G., 1991. $^{234}U/^{238}U$ mass spectrometry of corals: how accurate is the U–Th age of the last interglacial period? Earth Planet. Sci. Lett. 106, 169.
Hay, C.C., Morrow, E., Kopp, R.E., Mitrovica, J.X., 2012. Estimating the sources of global sea level rise with data assimilation techniques. Proc. Nat. Acad. Sci. 110, 3692–3699.
Hearty, P.J., Kindler, P., Cheng, H., Edwards, R.L.A., 1999. +20 m middle Pleistocene sea level highstand (Bermuda and the Bahamas) due to partial collapse of Antarctic ice. Geology 27, 375–378.
Hearty, P.J., Hollin, J.T., Neumann, A.C., O'Leary, M.J., McCulloch, M., 2007. Global sea-level fluctuations during the Last Interglaciation (MIS5e). Quat. Sci. Rev. 26, 2090–2112.
Israelson, C., Wohlfarth, B., 1999. Timing of the last-interglacial high sea level on the Seychelles Islands, Indian Ocean. Quat. Res. 51, 306.
Jouannic, C., Hantoro, W.S., Hoang, C.T., Fournier, M., Lafont, R., Ichtam, M.L., 1988. Quaternary raised reef terraces at cape Laundi, Sumba, Indonesia: geomorphological analysis and first radiometric Th/U and ^{14}C age determinations. In: Steneck, R.S., Choat, J.H., Barnes, D., Borowitzka, M.A. (Eds.), 6th Proceedings International coral reef symposium, vol. 2, pp. 441–447. Townsville, Australia.
Karner, D.B., Marra, F., 1998. Correlation of fluviodeltaic aggrada-tionsal sections with glacial climate history: a revision of the Pleistocene stratigraphy of Rome. Geol. Soc. Am. Bull. 110, 748–758.
Karner, D.B., Marra, F., 2003. $^{40}Ar/^{39}Ar$ dating of glacial termination V and the duration of marine isotopic stage 11. In: Droxler, A., Poore, R.Z., Burkle, L.H. (Eds.), Earth's Climate and Orbital Eccentricity: The Marine Isotope Stage 11, Geophysical Monograph 137. American Geophysical Union, pp. 61–68.
Karner, D.H., Renne, P.R., 1998. $^{40}Ar/^{39}Ar$ geochronology of Roman volcanic province tephra in the Tiber river valley: age calibration of middle Pleistocene sea-level changes. Geol. Soc. Am. Bull. 110, 740–747.
Kaufman, D.S., 1992. Aminostratigraphy of Pliocene-Pleistocene high sea-level deposits, Nome coastal plain and adjacent near shore area, Alaska. Geol. Soc. Am. Bull. 104, 40–52.
Kaufman, D.S., Brigham-Grette, J.K., 1993. Aminostratigraphic correlations and paleotemperature implications, Piocene-Pleistocene high sea-level deposits northwestern Alaska. Quat. Sci. Rev. 12, 21–33.
Kendall, R.A., Mitrovica, J.X., Milne, G.A., 2005. On post-glacial sea level: II. Numerical formulation and comparative results on spherically symmetric models. Geophys. J. Int. 161, 679–706.
Kopp, R.E., Mitrovica, J.X., Griffies, S.M., Yin, J., Hay, C.C., Stouffer, R.J., 2010. The impact of Greenland melt on local sea levels: a partially coupled analysis of dynamic and static equilibrium effects in idealized water-hosing experiments. Clim. Change 103, 619–625.
Kopp, R.E., Simons, F.J., Mitrovica, J.X., Maloof, A.C., Oppenheimer, M., 2009. Probabilistic assessment of sea level during the last interglacial. Nature 462, 863–867.
Kopp, R.E., Simons, F.J., Mitrovica, J.X., Maloof, A.C., Oppenheimer, M.A., 2013. Probabilistic assessment of sea level variations within the last interglacial stage. Geophys. J. Int. 193, 711–716.
Lambeck, K., Nakada, M., 1992. Constraints on the age and duration of the last interglacial period and on sea-level variations. Nature 357, 125–128.
Lambeck, K., Purcell, A., Dutton, A., 2011. The anatomy of interglacial sea levels: the relationship between sea levels and ice volumes during the last interglacial. Earth Planet. Sci. Lett. 315, 4–11.
Lambeck, K., Smither, C., Johnston, P., 1998. Sea level change, glacial rebound and mantle viscosity for northern Europe. Geophys. J. Int. 134, 102–144.
Lundberg, J., McFarlane, D.A., 2002. Isotope stage 11 sea-level in the Netherlands Antilles. Geol. Soc. Am. Program. Abstr. 34 (6), 31.
McCulloch, M.T., Mortimer, G., 2008. Applications of the 238U-230Th decay series to dating of fossil and modern corals using MC-ICPMS. Aust. J. Earth Sci. 55, 955.
McKay, N.P., Overpeck, J.T., Otto-Bliesner, B.L., 2011. The role of ocean thermal expansion in last interglacial sea level rise. Geophys. Res. Lett. 38. http://dx.doi.org/10.1029/2011GL048280.
McMurtry, G.M., Tappin, D.R., Sedwick, P.N., Wilkinson, I., Fietzke, J., Sellwood, B., 2007. Elevated marine deposits in Bermuda record a late Quaternary mega-tsunami. Sed. Geol. 200, 155–165.
Miller, K.G., Wright, J.D., Browning, J.V., Kulpecz, A., Kominz, M., Naish, T.R., Cramer, B.S., Rosenthal, Y., Peltier, W.R., Sisidian, S., 2012. High tide of the warm Pliocene: implications of global sea level for Antarctic deglaciation. Geology 40, 407–410.
Milne, G.A., Mitrovica, J.X., 1996. Postglacial sea-level change on a rotating Earth: first results from a gravitationally self-consistent sea-level equation. Geophys. J. Int. 126, F13–F20.
Mitrovica, J.X., Forte, A.M., 2004. A new inference of mantle viscosity based upon a joint inversion of convection and glacial isostatic adjustment data. Earth Planet. Sci. Lett. 225, 177–189.
Mitrovica, J.X., Tamisiea, M.E., Davis, J.L., Milne, G.A., 2001. Polar ice mass variations and the geometry of global sea level change. Nature 409, 1026–1029.
Mitrovica, J.X., Wahr, J., Matsuyama, I., Paulson, A., 2005. The rotational stability of an ice-age earth. Geophys. J. Int. 161, 491–506.
Mitrovica, J.X., Gomez, N., Morrow, E., Hay, C., Latychev, K., Tamisiea, M.E., 2011. On the robustness of predictions of sea level fingerprints. Geophys. J. Int. 187, 729–742.
Muhs, D.R., Pandolfi, J.M., Simmons, K.R., Schumann, R.R., 2012. Sea-level history of past interglacial periods from uranium-series dating of corals, Curaçao, Leeward Antilles islands. Quat. Res. 78, 157–169.
Muhs, D.R., Simmons, K.R., Kennedy, G.L., Ludwig, K.R., Groves, L.T., 2006. A cool eastern Pacific Ocean at the close of the last interglacial complex. Quat. Sci. Rev. 25, 235.
Muhs, D.R., Simmons, K.R., Kennedy, G.L., Rockwell, T.K., 2002a. The last interglacial period on the Pacific Coast of North America: timing and paleoclimate. Geol. Soc. Am. Bull. 114, 569–592.
Muhs, D.R., Simmons, K., Schumann, R., Halley, R.B., 2011. Sea-level history of the past two interglacial periods: new evidence from U-series dating of reef corals from south Florida. Quat. Sci. Rev. 30, 570.
Muhs, D.R., Simmons, K.R., Steinke, B., 2002b. Timing and warmth of the last interglacial period: new U-series evidence from Hawaii and Bermuda and a new fossil compilation for North America. Quat. Sci. Rev. 21, 1355.
Muhs, D.R., Wehmiller, J.F., Simmons, K., York, L.L., 2004. Quaternary sea-level history of the United States. In: Gillespie, A.R., Porter, S.C., Atwater, B.F. (Eds.), The Quaternary Period in the United States. Elsevier, Amsterdam, pp. 147–184.
Murray-Wallace, C.V., 2002. Pleistocene coastal stratigraphy, sea-level highstands and neotectonism of the southern Australian passive continental margin – a review. J. Quatern. Sci. 17, 469–489.
O'Leary, M.J., Hearty, P.J., McCulloch, M.T., 2008a. U-series evidence for widespread reef development in Shark Bay during the last interglacial. Palaeogeogr. Palaeoclimatol. Palaeoecol. 259, 424.
O'Leary, M.J., Hearty, P.J., McCulloch, M.T., 2008b. Geomorphic evidence of major sea- level fluctuations during marine isotope substage-5e, Cape Cuvier, Western Australia. Geomorphology 102, 595.
O'Leary, M.J., Hearty, P.J., Thompson, W.G., Raymo, M.E., Mitrovica, J.X., Webster, J.M., 2013. Ice sheet collapse following a prolonged period of stable sea level during the last interglacial. Nat. Geosci.. http://dx.doi.org/10.1038/ngeo1890.
Olson, S.L., Hearty, P.J., 2009. A sustained +21 m sea level highstand during MIS 11 (400 ka): direct fossil and sedimentary evidence from Bermuda. Quat. Sci. Rev. 28, 271–285.
Omura, A., Maeda, Y., Kawana, T., Siringan, F.P., Berdin, R.D., 2004. U-series dates of Pleistocene corals and their implications to the paleo-sea levels and the vertical displacement in the Central Philippines. Quat. Int. 115–116, 3–13.
Ota, Y., Omura, A., 1992. Contrasting styles and rates of tectonic uplift of coral reef terraces in the Ryukyu and Daito Islands, southwestern Japan. Quat. Int. 15–16, 17–29.
Peltier, W.R., 2004. Global glacial isostasy and the surface of the ice-age Earth: the ICE-5G (VM2) model and GRACE. Ann. Rev. Earth Planet. Sci. 32, 111–149.
Pirazzoli, P.A., Radtke, U., Hantoro, W.S., Jouannic, C., Hoang, C.T., Causse, C., Borel Best, M., 1993. A one-million-year-long sequence of marine terraces on Sumba Island, Indonesia. Mar. Geol. 109, 221–236.
Plag, H.-P., Jüttner, H.U., 2001. Inversion of global tide gauge data for present-day ice load changesProceedings of the Second International Symposium on Environmental Research in the Arctic and Fifth Ny-Alesund Scientific Seminar. Mem. Nat. Inst. Polar Res. 54, 301–318.
Pushgar, V.S., Roof, S.R., Hopkins, D.M., Brigham-Grette, J., 1999. Paleogeographic and paleoclimatic significance of diatoms from Middle Pleistocene marine and

glaciomarine deposits on Baldwin Peninsula, northwestern Alaska. Palaeogeogr. Palaeoclimtol. Palaeoecol. 152, 67–85.
Raymo, M.E., Mitrovica, J.X., O'Leary, M.J., Deconto, R.M., Hearty, P.J., 2011. Departures from eustasy in Pliocene sea-level records. Nat. Geosci. 4, 328–332.
Raymo, M., Mitrovica, J.X., 2012. Collapse of polar ice sheets during the stage 11 interglacial. Nature 483, 453–456.
Roberts, D.L., Karkanas, P., Jacobs, Z., Marean, C.W., Roberts, R.G., 2012. Melting ice sheets 400,000 yr ago raised sea level by 13 m: past analogues for future trends. Earth Planet. Sci. Lett. 357, 226–237.
Rowley, D.B., Forte, A.M., Moucha, R., Mitrovica, J.X., Simmons, N.A., Grand, S.P., 2013. Dynamic topography change of the eastern United States since 3 million years ago. Science 340, 1560–1563.
Schellmann, G., Radtke, U., 2004. A revised morpho- and chronos-tratigraphy of the late and middle Pleistocene coral reef terraces on Southern Barbados (West Indies). Earth Sci. Rev. 64, 157–187.
Solomon, S.D., Manning, M., Qin, D. (Eds.), 2007. Climate Change 2007: The Physical Basis 4th Assessment Report. IPCC, Cambridge Univ. Press, Cambridge.
Speed, R.C., Cheng, H., 2004. Evolution of marine terraces and sea level in the last interglacial, Cave Hill, Barbados. Geol. Soc. Am. Bull. 116, 219.
Stirling, C.H., Esat, T.M., Lambeck, K., McCulloch, M.T., 1998. Timing and duration of the last interglacial: evidence for a restricted interval of widespread coral reef growth. Earth Planet. Sci. Lett. 160, 745.
Stirling, C.H., Esat, T.M., McCulloch, M.T., Lambeck, K., 1995. High-precision U-series dating of corals from Western Australia and implications for the timing and duration of the last interglacial. Earth Planet. Sci. Lett. 135, 115.
Stone, E.J., Lunt, D.J., Annan, J.D., Hargreaves, J.C., 2013. Quantification of the Greenland ice sheet contribution to last interglacial sea-level rise. Clim. Past. Discuss. 8, 2732–2776.
Tamisiea, M.E., Mitrovica, J.X., Milne, G.A., Davis, J.L., 2001. Global geoid and sea level changes due to present-day ice mass fluctuations. J. Geophys. Res. 106, 30849–30863.
van Hengstum, P., Scott, D.B., Javaux, E., 2009. Foraminifera in elevated Bermudian caves provide further evidence for +21 m eustatic sea level during Marine Isotope Stage 11. Quat. Sci. Rev. 28, 1850–1860.
Walter, R.C., et al., 2000. Early human occupation of the Red Sea coast of Eritrea during the last interglacial. Nature 405, 65.
Zhu, Z.R., et al., 1993. High-precision U-series dating of Late Interglacial events by mass spectrometry: Houtman Abrolhos Islands, Western Australia. Earth Planet. Sci. Lett. 118, 281.